Synthesis and Electrochemical Evaluation of Pd_8Sb_3 and PtSb Ordered Intermetallics Toward the Oxygen Reduction and Hydrogen Oxidation Reactions

by

Hamdan Ahmed Alghamdi

A thesis submitted to Johns Hopkins University in conformity with the requirements for the degree of Master of Science in Engineering

Baltimore, Maryland

May 2019

Abstract

Energy consumption and chemical conversion from nonrenewable sources such as fossil fuels greatly affect the environment and it is a leading global issue. Electrochemical conversion once mature could pose as an alternative technology, yet, electrode materials require further development to increase efficiencies and reduce cost. While precious metals exhibit high activities and stability as electrocatalyst, their cost and the possibility of activity enhancement led many to finding alternative materials. Alloying precious metals with non-precious metals to reduce the amount of precious metals used and hence total cost has also shown to increase activities in some cases. In this work, two ordered intermetallics of Pd_8Sb_3 and PtSb are synthesized and evaluated toward oxygen reduction and hydrogen oxidation reactions, respectively.

Single phase Pd_8Sb_3 ordered intermetallic supported on carbon is successfully synthesized at a low temperature of 250°C. The electrochemical oxygen reduction activity of as-synthesized Pd_8Sb_3 in alkaline conditions closely matches Pd efficiency with ~ 1 mA/cm^2. The activity of Pd_8Sb_3, however, is improved to 1.65 mA/cm^2 upon annealing to 500°C. Additionally, dominant single phase PtSb/C electrocatalyst is synthesized and its efficiency towards the hydrogen oxidation reaction in alkaline conditions is evaluated. PtSb exhibits better specific activity for the reaction with kinetic currents of 13 and 4 mA/cm^2 at 100 and 10 V.

Advisor: Dr. Shoji. A. Hall

Reader: Dr. Wang Chao

Table of Contents

List of Tables

List of Figures

Introduction

Since the industrial revolution, the use of non-renewables such as fossil fuels for energy generation and consumption has led to a tremendous increase in greenhouse gases. These gases trap earth's heat and lead to an increase in global temperatures which threaten many lifecycles on it. Researchers in many fields are developing technologies that are more environment friendly utilizing renewable sources such as wind and sunlight. However, these technologies are not mature enough to replace the capital infrastructure built for the use of fossil fuels. An alternative to fossil fuels is water. Water is an abundant raw material and once it is split into its molecular constituents, oxygen and hydrogen, can be burned to form water again releasing energy.

Water formation at a molecular level happens via two parallel reactions: oxygen reduction reaction (ORR) and hydrogen oxidation reaction (HOR). In practical situations, the reactions would take place simultaneously in a fuel cell and can be studied individually using the rotating disk electrode (RDE) method. While ORR and HOR can occur in acidic and basic conditions, the latter is at interest due to the possibility of corrosion and materials stability in acidic conditions. There are two mechanisms for oxygen reduction half reaction: four-electron pathway (Equation 1) and two-electron pathway (Equations 2–3). For energy generation (i.e. electrical current), the direct reduction of oxygen via the four-electron pathway is preferable whereas the formation of peroxide in the two-electron pathway can be useful in oxidation of chemicals into more valuable chemicals.

ORR four-electron pathway: $O_2 + H_2O + 4e^- \rightarrow 4OH^-$ (1)

ORR two-electron pathway: $O_2 + H_2O + 2e^- \rightarrow HO_2^- + OH^-$ (2)

$HO_2^- + H_2O + 2e^- \rightarrow 3OH^-$ (3)

HOR: $H_2 \rightarrow 2H^+ + 2e^-$ (4)

In general, precious metals are highly durable and active toward electrochemical reactions. For example, platinum has shown to be very efficient and stable for HOR [1] and similarly for palladium toward ORR [2]. The chemical and physical properties of metals such as Pd, differ from bulk [3, 4], single crystals [5, 6, 7, 8], to nanoparticles [9, 10, 11, 12, 13, 14]. Nanoparticles supported on carbon in particular gained the highest interest in recent years in the development of high performing electrocatalysts. Therefore, Pt/C and Pd/C nanoparticles are considered prototype catalysts for the HOR and ORR, respectively. Nevertheless, due to their viability and cost, they are undesirable for practical applications, and the need of developing alternative efficient and cheap electrocatalysts is increasing. Intermetallic nanoparticles have shown to be a promising candidate in this field. For instance, ordered intermetallics such as Pt_3Ni and Pd_3Bi have demonstrated to be superior to Pt and Pd in ORR activity [15, 16]. Ir_3PdRu_6 on the other hand showed a significant activity enhancement toward HOR compared to Pt [17].

Metals of the Pnictogen group (i.e. group 15) of the periodic table has some attraction in the development of ordered intermetallics and their application in electrochemical reactions. Reactions such as oxygen reduction, hydrogen evolution, formic acid oxidation, methanol oxidation, and ethanol oxidation on intermetallic systems containing bismuth have been studied [18]. In addition, Pt–Sb intermetallics have shown better performance for many oxidation reactions and PtSb phase in particular has shown

double the specific activity for HOR in acidic conditions [19]. Other Pt–Sb intermetallics have not been investigated thoroughly particularly for electrochemical reduction reactions [6] and there are no available reports on Pd-Sb intermetallics for electrochemical ORR or HOR. In this work, Pd_8Sb_3 are PtSb successfully synthesized and their activities toward electrochemical ORR and HOR in alkaline conditions are investigated.

Experimental Methods and Techniques

Chemicals and Materials

The chemicals platinum(II) acetylacetonate (Sigma Aldrich, 99.7%), palladium (II) nitrate hydrate (Alfa Aesar, 99.8%), antimony (III) acetate (Sigma Aldrich, 99.99%), polyvinylpyrrolidone (PVP, Alfa Aesar), carbon black (FuellCellStore , Vulcan XC−72R), sodium borohydride (H_4BNa, Sigma Aldrich, 99.99%), isopropanol (IPA, Sigma Aldrich, ≥99.5), triethylene glycol (TEG, Alfa Aesar, 99%), oleic acid (Fisher Chemical), nafion (5 wt.% in alcohol) are used to synthesis the ordered intermetallic materials. Pd/C (Premetel Co., 40 wt.%) and Pt/C (TKK, 47.1 wt.%) are used as reference catalysts. Potassium hydroxide (Alfa Aesar, 99.98% metal basis) and ultra-high purity water is used throughout the experimentation and is generated using Milli−Q water purification system (Fisher Scientific, 18.2 MΩ−cm resistivity, <5 ppb TOC). All glassware used in the synthesis were stored in a basic solution prior to usage then adequately washed with water to eliminate unreacted residual chemicals.

Synthesis of Ordered Pd_8Sb_3 Intermetallics

Pd_8Sb_3/C was synthesized using a protocol similar to the one described in [20]. Initially, two mixtures are prepared in parallel. For the first mixture, 0.57 mmol of Pd (II) nitrate hydrate, 0.20 mmol of Sb (III) acetate, 150 mg PVP, and 128 mg Vulcan (targeted metal loading 40 wt.%) are dissolved and mixed in 20 mL TEG. The mixture is then sonicated for 1 hour and transferred to a three-nick flask. While stirring, the mixture is

heated to 150°C and put under vacuum for a few minutes, and then the headspace is put under Ar. Following that, the temperature is set to 260°C. The second mixture consisted of 50 mg of H_4BNa dissolved in 10 mL TEG and also sonicated for 1 hour. Once the temperature in the flask reaches 260°C, the second mixture containing the reducing agent (i.e. H_4BNa) is injected into the flask and the system is let to react for 45 minutes. After the system has reacted, it is let to cool to room temperature and centrifuged and washed twice with a mixture of IPA and H_2O and then twice with IPA. Finally, the product is dried at 80°C overnight.

Synthesis of Ordered PtSb Intermetallics

The synthesis of PtSb/C is similar to [21] recipe with adjustments. In summary, 150 mg of Vulcan (targeted metal loading 40 wt.%) is suspended in 25 mL TEG and is purged with Ar for 20 minutes and then sonicated for 30 minutes. The suspension is then transferred to a three-neck flask connected to a reflux system. 0.32 mmol of Sb (III) acetate and 200 mg PVP are added to the flask. While stirring, the flask is sealed and degassed at 150°C for a few minutes and then heated to 210°C to react for 16 hours under reflux. Before the end of the reaction time, 0.32 mmol of Pt (II) acetylacetonate is dissolved in a solution containing 25 mL TEG and 6.25 mL oleic acid that is purged with Ar for 20 minutes. The Pt precursor solution is then added to the reacting flask dropwise over a period of 1 hour. The system is then sealed and let to react for 48 hours at 250°C. Post reaction washing and drying procedures are similar to Pd_8Sb_3.

X-ray diffraction is employed for crystal phase identification. The Inorganic Crystal Structure Database (ICSD) IDs of the Pd_8Sb_3 and PtSb crystals used are 655017 and 16969, respectively. Pourbaix diagrams are generated using pymatgen [22].

Electrochemical Evaluation

Sample Preparation

The Rotation Disk Electrode (RDE) method is used to conduct electrochemical testing for all samples. To prepare the samples for the use of RDE, ink suspensions of the electrocatalysts are prepared by suspending 10 mg of the catalyst in 2.4 mL IPA, 0.6 mL H_2O, and 20 µL nafion. The suspension is then sonicated for at least 30 minutes. Depending on the targeted roughness factor, ink volume of the suspension in the range of 1–10 µL is casted on a finely polished glassy carbon (Ø=0.5 cm) and left to dry in air for 30 minutes.

Electrochemical Testing

Autolab PGSTAT 204 (Eco–Chemie) potentiostat/galvanostat is used to conduct the electrochemical tests and is controlled by Nova® software. Electrochemical measurements are collected using a 300 mL Teflon cell with graphite rod and Hg/HgO electrode (CH Instruments) for which are used as counter and reference electrodes. Hg/H_2SO_4 electrode (CH Instruments) is used as a reference electrode for testing in 0.1 M $HClO_4$. All potentials collected ($E_{ref,p}$) by the reference electrode are converted to the reversible hydrogen electrode (RHE) using Equation 5 where E^o_{ref} is 0.140 V for Hg/HgO

and 0.658 V for Hg/H_2SO_4. A glassy carbon is used as the support for the working electrode at which a catalyst ink is casted.

$$E_{RHE,p} = E_{ref,p} + E^{o}_{ref} + 0.059\ pH \tag{5}$$

Prior to conducting each electrochemical test, conditioning of the catalyst surface is performed by cycling the potential 100 times from 0 to 1.2 V vs. RHE (scan rate: 100 mV/s, step: 1 mV) in Ar saturated electrolyte. The conditioning step precedes all any electrochemical testing in this work to ensure electrode cleanness and electrical current stability. A cyclic voltammogram (CV) is collected under Ar (scan rate: 10 mV/s, step: 1 mV) unless stated otherwise. ORR and HOR are performed by purging the reactant gas (either O_2 or H_2) in the electrolyte for at least 30 minutes. Once the solution is saturated, the reactions are performed by conducting a linear sweep voltammogram (LSV) from 0 to 1.2 V vs. RHE (scan rate: 5 mV/s, step: 0.2 mV). At the completion of each reaction, the electrochemical active surface area (ECSA) is determined via CO oxidation/stripping by saturating the electrolyte with CO and holding the potential at 0.2 V vs. RHE for 10 minutes. After that and still while the potential is held at 0.2 V, the system is purged with Ar for 30 minutes and then a CV is collected for three scans (scan rate: 50 mV/s, step: 5 mV) to allow for control scan subtraction.

Knowing the scan rate (r) and calculating the peak area of CO stripping (PA_{CO}) with the assumption of 1 e^- transfer and stripping charges (η) of 484 and 420 $\mu C/cm^2$ (Pt and Pd, respectively), the ECSA is calculated as Equation 5.

[redacted] (5)

A roughness factor is a ratio of the ECSA and the geometrical area. For the ORR, the targeted roughness factor is 10 whereas for HOR is 2. Surface area specific activities (SA_p) are calculated using Equation 6 and reaction LSVs. The Mass transport corrected current ($I_{k,p}$) at any potential (p) is computed using the LSV test where I_{lim} is the diffusion-limiting current and I_p is the current at potential (p).

[redacted] (6)

Equations 7-9 represent Koutecký–Levich (KL) equation and is utilized in this work to calculate the number of electrons (n) involved in the ORR. The measured/observed current at steady state (J) is composed of mass-transport corrected (J_L) and kinetic (J_K) currents. By plotting $1/J$ vs. $1/\omega^{1/2}$ where ω is the rotation rate, Levich constant B (unit: $A/cm^2/rpm^{1/2}$) is determined. The values of O_2 concentration (C_o), diffusion coefficient of O_2 in 0.1 M KOH (D_o), and kinematic viscosity (v) assumed in the analysis are 1.21×10^{-6} mol/cm^3, 1.93×10^{-5} mol/cm^3 [23], and 1.09×10^{-2} cm^2/s [24], respectively. F is the Faraday constant (96485 A·s/mol).

[redacted] (7)

[redacted] (8)

[redacted] (9)

Results and Discussion

Evaluation of Pd_8Sb_3/C Electrocatalytic Activity for the Oxygen Reduction Reaction

The intermetallic phase of the synthesized electrocatalyst has been confirmed to be Pd_8Sb_3/C using x–ray diffraction as shown in Figure 1. The main features of the experimental pattern located at 39.5, 40.3, 41.2° and other detected features are in agreement to the simulated pattern which identifies the bulk crystallographic phase as Pd_8Sb_3. The peak at 21.5° is due to the presence of carbon black support.

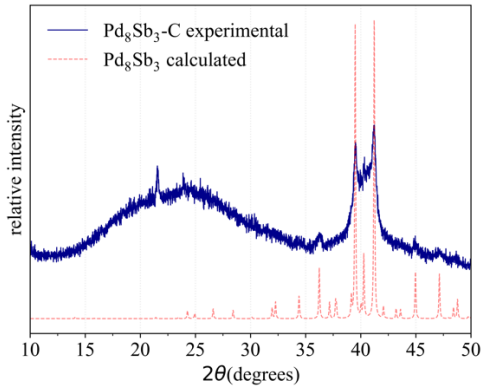

Figure 1. Experimental and simulated XRD patterns of Pd_8Sb_3.

Figures 2A–B show the conditioning CVs of Pd/C and Pd_8Sb_3/C, respectively. While conditioning, Pd/C does not show major changes up to 100 scans indicating surface cleanness and stability. On the other hand, changes in the Pd_8Sb_3/C sample could be due to surface cleaning and/or restructuring. The appearance of the oxide feature at 0.64 V in the positive scan of Pd_8Sb_3/C and the shift of Pd reduction feature to 0.72 V in the negative scan is most likely to be due to Pd enrichment in the surface. The extent of similarities of redox features of Pd/C and Pd_8Sb_3/C can be seen in the slow scan CV as shown in Figure

2C. Major differences in the features are the peak shift from 0.33 V in Pd to 0.43 V in Pd_8Sb_3 and the drastic suppression of H_{upd} current in Pd_8Sb_3 compared to Pd. Figure 2D shows the ORR RDE measurements for the samples. Pd/C and Pd_8Sb_3/C exhibits similar ORR catalytic activities where the saturation current reached is ~7.6 mA/cm^2 for both samples.

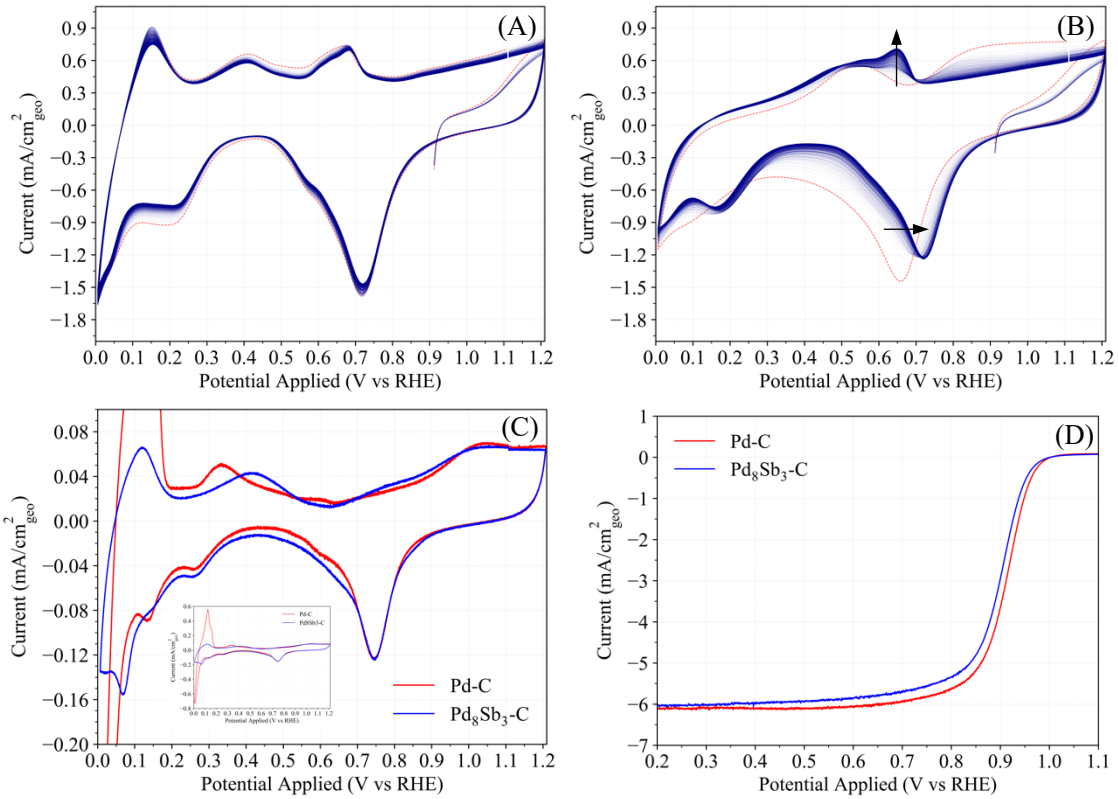

Figure 2. (A) and (B): Conditioning CVs of Pd/C (A) and Pd_8Sb_3/C (B) in Ar–saturated solution at 100 mV/s. Color intensity increases from scan number 1 to 100. **(C):** Cyclic voltammogram in Ar for Pd/C and Pd_8Sb_3/C at 10 mV/s. Inset: full range CV. **(D):** ORR for Pd/C and Pd_8Sb_3/C at 1600 rpm and 5 mV/s. All conducted in 0.1 M KOH electrolyte.

From Figure 2D, the half-way potential of Pd_8Sb_3/C is 13 mV slightly lower than that of Pd/C (0.91 V). However, it is observed that values of half–way potentials are

sensitive to catalyst loading and thus not sufficiently reliable in quantitative comparisons. One method to quantitively compare electrocatalytic activities is by computing specific activities. The calculated ECSA and roughness factor of Pd/C are 2.2 cm^2 and 11 whereas for Pd_8Sb_3/C are 1.5 cm^2 and 8 as illustrated in Figure 3. Those values are within a comparable and adequate range to get insight exclusively to the intrinsic behavior of the catalytic system.

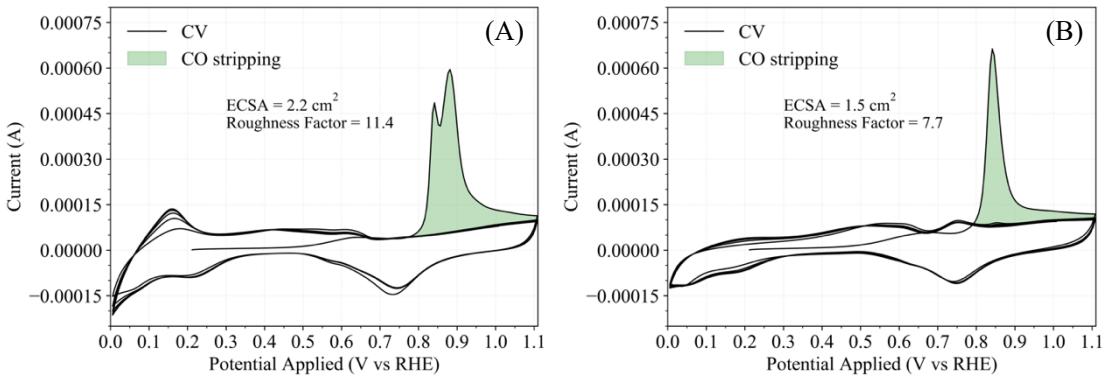

Figure 3. CO stripping CV of **A:** Pd/C and **B:** Pd_8Sb_3/C (B) in Ar saturated 0.1 M KOH at scan rate of 50 mV/s.

The ORR specific activity of Pd_8Sb_3/C in the range 0.8–1.0 V greatly roughly resembles that of Pd/C as shown in Figure 4A. The measured specific activities for Pd/C and Pd_8Sb_3/C at 0.9 V are 1.0 and 0.95 mA/cm^2_{metal}, respectively. At a higher overpotential of 0.85 V, the specific activities are 3.82 and 3.85 mA/cm^2. The high resemblance of Pd_8Sb_3/C in the main features and catalytic performance to that of Pd/C after conditioning could be explained by surface restructuring to be highly rich in Pd. ORR Rotation dependent linear sweep voltammograms (LSV) and steady-state currents at different potentials are shown in Figure 4B. From the steady state results, the average number of electrons involved in a single reaction is calculated using KL equation discussed in the

experimental section and found to be 4.3 (Figure 4C) in the range of 0.5–0.8 indicating a four-electron pathway for the ORR. The calculated Tafel slopes of Pd_8Sb_3 for ORR are 47 and 195 mV/dec in the potential regions 0.85–0.95 and 0.58–0.75 V, respectively as shown in Figure 4D. The exchange current density (I_o) is calculated to be 1.03×10^{-6} mA/cm^2. The Tafel slopes of the Pd_8Sb_3 intermetallic are close to that of Pd references as shown in Table 1. The difference in the specific activities to the references could be due to experimental conditions such as catalyst loading affecting roughness and current measurement type (i.e. steady state or LSV). The measured specific activities in Figure 4A are calculated using LSV collected at slow scan rate of 5 mV/s and the reactions reach a kinetic limitation with a clear plateau in the potential region 0.20–0.40 V. This method allows for the computation of kinetic currents, $I_{k,p}$, as shown in Equation 6.

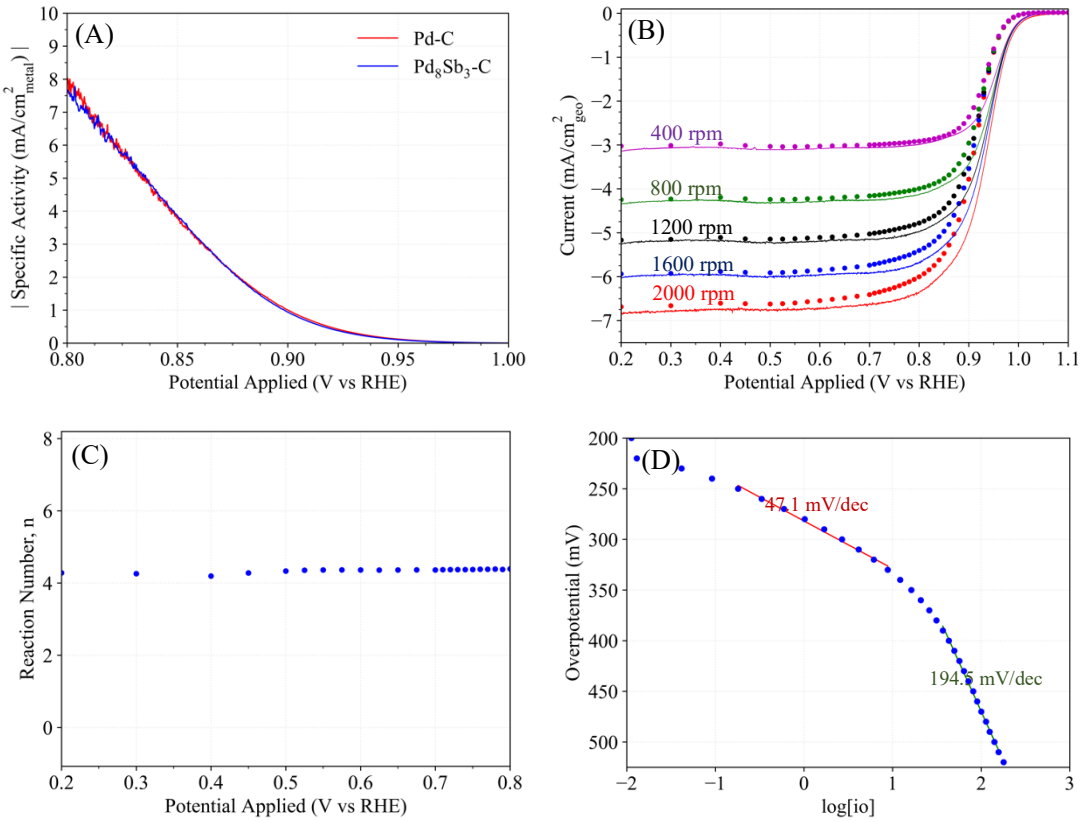

Figure 4. A: ORR Specific activities of Pd/C and Pd_8Sb_3/C normalized to ECSA at 1600 rpm. **B:** LSV (lines, 20 mV/s) and steady state (dots, potential held for 30s at each point) ORR measurements at different rotation rates. **C:** Reaction electron number of Pd_8Sb_3/C for ORR calculated using KL equation. **D:** Tafel plot of Pd_8Sb_3/C at 1600 rpm. All conducted in 0.1 M KOH electrolyte.

Table 1. Specific activities for ORR and Tafel slopes of Pd_8Sb_3/C compared to references of Pd/C in 0.1 M KOH and at 1600 rpm. a, b, and c: potential ranges of (0.85–0.95), (0.73–0.85), and (0.58–0.75) V vs. RHE

Catalyst	**SA at 0.85 V (mA/cm^2)**	**SA at 0.9 V (mA/cm^2)**	**Tafel Slopes (mV/dec)**
Pd/C [25]	--	0.39	52[a], 133[b]
Pd/C [26]	1.79	0.77	55[a], 193[c]
Pd/C (This work)	3.82	1.00	--
Pd_8Sb_3/C (This work)	3.85	0.95	47[a], 195[c]

From the phase diagram of Pd–Sb [27], the melting point of the Pd–rich Pd_8Sb_3 is very high indicating its high stability compared to Sb–rich phases. However, stability could differ under electrochemical testing conditions and therefore a Pourbaix diagram is utilized to investigate its stability. From Figure 5, at high pH values, Sb atoms on the surface are susceptible to oxidation and the formation of free ions thus jeopardizing the intermetallic surface structure. As Sb atoms get oxidized, the surface becomes richer in Pd until no more Sb atoms are available on the surface. This surface restructuring could be an explanation to the changes in features during conditioning and the similarities of Pd_8Sb_3 and Pd CVs and it can also explain the highly comparable catalytic efficiencies for ORR.

In the XRD results of Pd_8Sb_3/C shown in Figure 1, the low intensity of diffraction signals could indicate low crystallinity. Therefore, Pd_8Sb_3 is furtherly treated by annealing at 500°C for three hours. Annealing the sample has improved its specific activity (Figure 6A) from 0.95 to 1.65 mA/cm^2 at 0.9 V and from 3.85 to 6.25 mA/cm^2 at 0.85 V. It is not

yet completely understood why this activity enhancement occurs, and it is currently a work in progress.

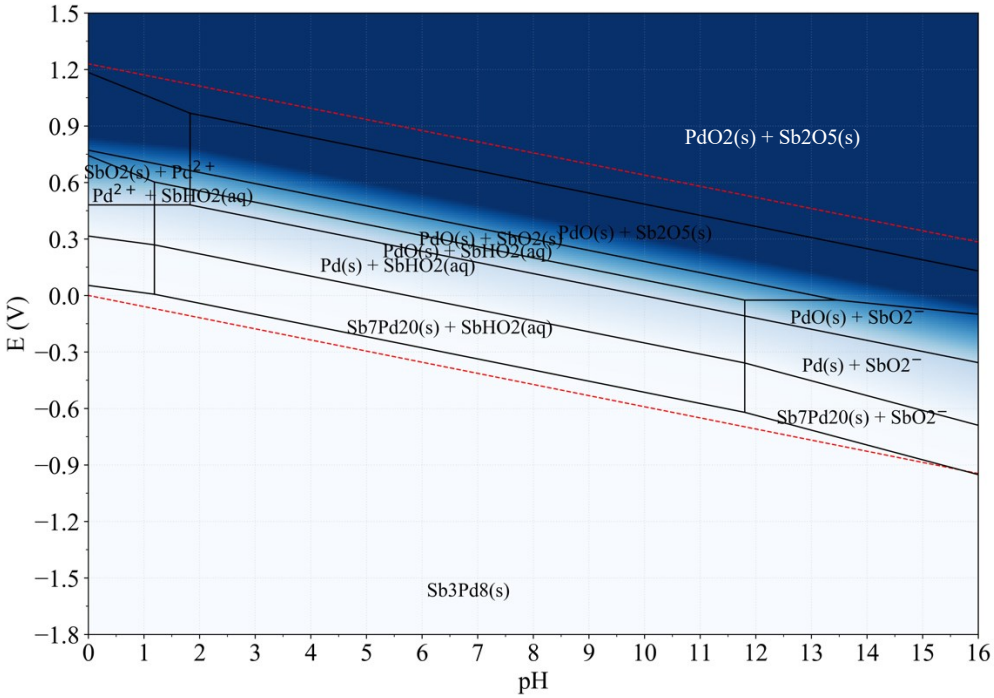

Figure 5. Pourbaix diagram of Pd_8Sb_3. Shading intensity indicate instability from 0 (light, stable) to 1 eV/atom and higher (dark, unstable). The red dashed lines represent the OER and HER potential profiles.

Accelerated durability tests (ADT) have not been conducted to evaluate the stability of the samples, but initial exploration of Pd_8Sb_3 electrochemical activity in alkaline solution proved its relative stability to Pd. On the other hand, Pd has been shown to be unstable in acidic conditions under electrochemical testing and could result either in the formation of inactive species on the catalyst surface [28] or the dissolution of metal [29, 30]. It is observed as shown in Figure 7 that Pd_8Sb_3 exhibits staggering instability in 0.1 M $HClO_4$

(pH 1). In less than 100 CV scans, the catalyst electrochemical features seem to completely disappear, and the ORR activity afterwards is greatly suppressed hence not worth showing. The instability could be a result of both metals Pd and Sb dissolving in the solution.

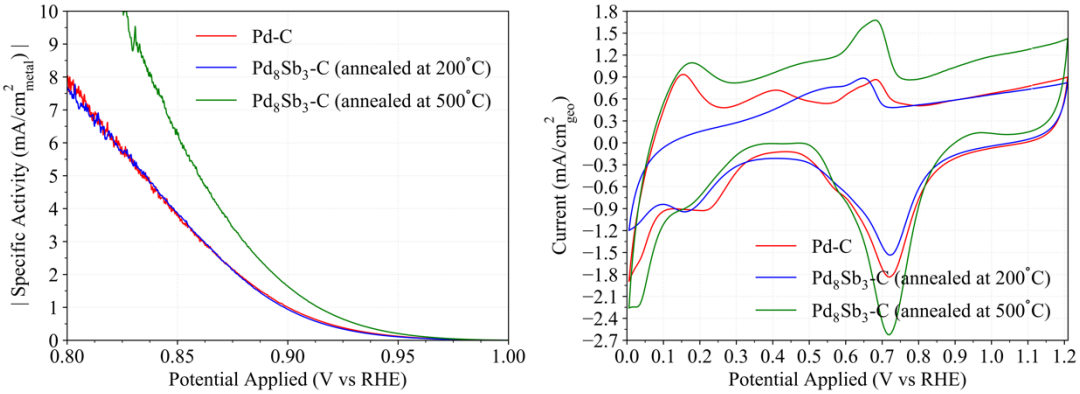

Figure 6. A: Effect of annealing at 500°C in the ORR specific activity of Pd_8Sb_3 in 0.1 M KOH. **B**: CV comparison of the Pd-C and Pd_8Sb_3-C (annealed and non-annealed) in 0.1 M KOH at 100 mV/s.

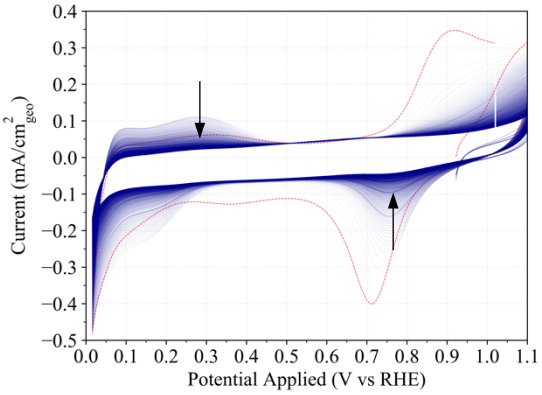

Figure 7. Conditioning CV of Pd_8Sb_3/C in 0.1 M $HClO_4$ (pH 1) at 100 mV/s and 1600 rpm.

Evaluation of PtSb/C Electrocatalytic Activity for the Hydrogen Oxidation Reaction

The collected diffraction pattern of PtSb/C resembles the simulated pattern of the targeted crystal phase PtSb. In the XRD results shown in Figure 8A, diffraction peaks at 25.0, 29.9, 41.6, and 43.8° are indicative of the presence of a dominant phase PtSb while peaks at 24, 27.8, 31.1, 34, 40.1, and 46.9° are due to contribution of $PtSb_2$ phase. Using the Rietveld method [31], the calculated composition of $PtSb_2$ in the synthesized catalyst is estimated to be 10%. The as−synthesized PtSb does not seem to undergo surface restructuring while conditioning as the observed features in the CV (Figure 8B) only intensify with number of scans to a certain extent. The increase in observed current could be due to surface sanitization.

In general, the redox features of Pt are more pronounced than PtSb as shown in Figure 8C. In contrast to Pd_8Sb_3 with respect to Pd, PtSb has a higher H_{upd} currents than Pt. The HOR profiles of PtSb/C and Pt/C (Figure 8D) are quite similar and the diffusion limited current for both is ~ 2.8 mA/cm^2_{geo}. Nevertheless PtSb/C performs better at potentials less than the saturation potential at 0.3 V vs. RHE.

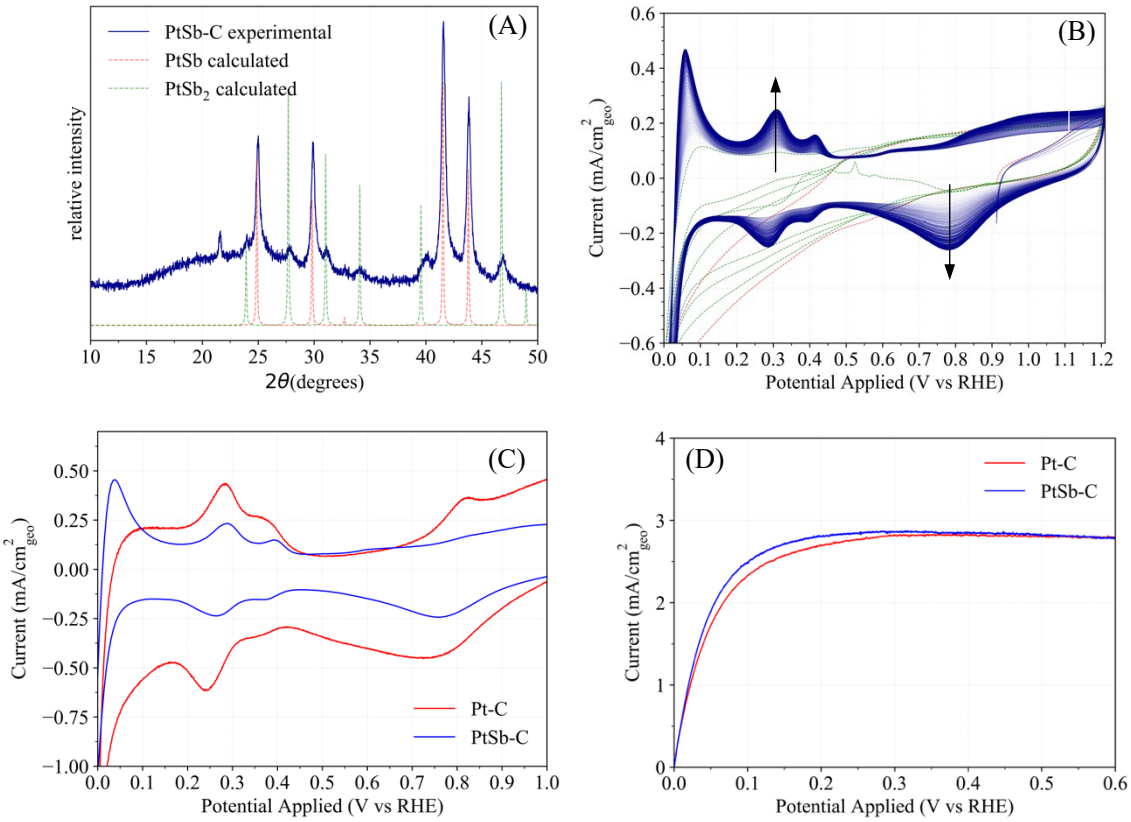

Figure 8. A: Experimental and simulated XRD patterns of PtSb. **B:** Conditioning of PtSb/C in Ar–saturated solution at 100 mV/s. Color intensity increases from scan number 1 to 100. The dashed red line is the first scan (break-in) and the green dashed lines are the next 3 scans. **C:** Cyclic voltammogram (CV) in Ar of stable Pt/C and PtSb/C after conditioining at 100 mV/s. **D:** HOR of Pt/C and PtSb/C at 1600 rpm and 5 mV/s. All conducted in 0.1 M KOH electrolyte.

PtSb/C shows a better performance than Pt/C in the HOR where at relatively high overpotentials such as 100 mV, the specific activities for PtSb/C and Pt/C are 13 and 7 mA/cm^2 as shown in Figure 9A. Whereas at a lower overpotential (10 mV), the activities are 4 and 3 mA/cm^2. Even though PtSb has similar CV to Pt and stability to Pd_8Sb_3 as shown in the Pourbaix diagram in Figure 9B, the catalytic activity of PtSb is higher and

not comparable to Pt. A possible explanation is the increase of H adsorption and desorption in PtSb compared to Pt.

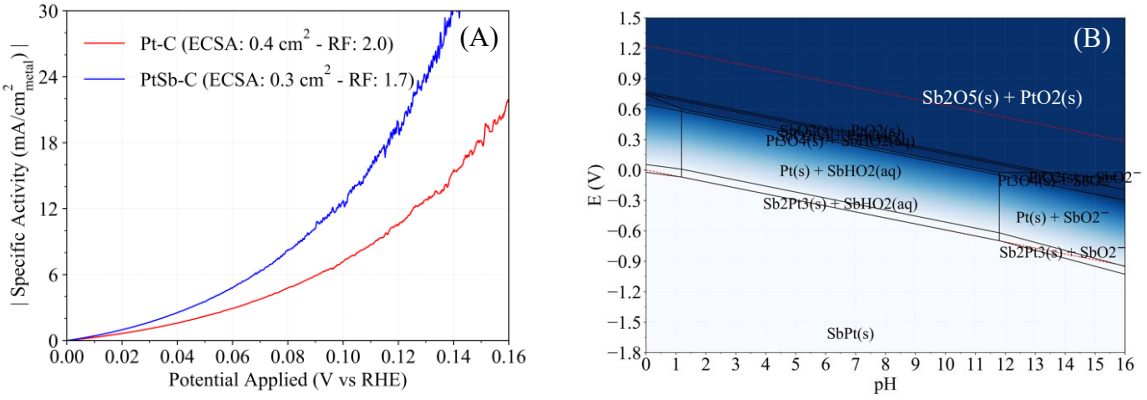

Figure 9. A: HOR Specific activities of Pt/C and PtSb/C normalized to ECSA. **B:** Pourbaix diagram of PtSb. Shading intensity indicate instability from 0 (light, stable) to 1 eV/atom and higher (dark, unstable). The red dashed lines represent the OER and HER potential profiles.

References

[1] Sheng, W.; Myint, M.; Chen, J. G.; Yan, Y. Correlating the Hydrogen Evolution Reaction Activity in Alkaline Electrolytes with the Hydrogen Binding Energy on Monometallic Surfaces. Energy & Environmental Science 2013, 6 (5), 1509.

[2] Shao, M.; Chang, Q.; Dodelet, J.-P.; Chenitz, R. Recent Advances in Electrocatalysts for Oxygen Reduction Reaction. Chemical Reviews 2016, 116 (6), 3594–3657.

[3] Nagle, L. C.; Garbarino, S.; Burke, D. Active Site and Electrocatalytic Behavior at Palladium Electrode Surfaces; ECS, 2010.

[4] Pan, W.; Zhang, X.; Ma, H.; Zhang, J. Electrochemical Synthesis, Voltammetric Behavior, and Electrocatalytic Activity of Pd Nanoparticles. The Journal of Physical Chemistry C 2008, 112 (7), 2456–2461.

[5] Kondo, S.; Nakamura, M.; Maki, N.; Hoshi, N. Active Sites for the Oxygen Reduction Reaction on the Low and High Index Planes of Palladium. The Journal of Physical Chemistry C 2009, 113 (29), 12625–12628.

[6] Wan, L.-J.; Suzuki, T.; Sashikata, K.; Okada, J.; Inukai, J.; Itaya, K. In Situ Scanning Tunneling Microscopy of Adsorbed Sulfate on Well-Defined Pd(111) in Sulfuric Acid Solution. Journal of Electroanalytical Chemistry 2000, 484 (2), 189–193.

[7] Hoshi, N.; Kagaya, K.; Hori, Y. Voltammograms of the Single-Crystal Electrodes of Palladium in Aqueous Sulfuric Acid Electrolyte: Pd(S)-[n(111)×(111)] and Pd(S)-[n(100)×(111)]. Journal of Electroanalytical Chemistry 2000, 485 (1), 55–60.

[8] Kibler, L.; Cuesta, A.; Kleinert, M.; Kolb, D. In-Situ STM Characterisation of the Surface Morphology of Platinum Single Crystal Electrodes as a Function of Their Preparation. Journal of Electroanalytical Chemistry 2000, 484 (1), 73–82.

[9] Shao, M. Palladium-Based Electrocatalysts for Hydrogen Oxidation and Oxygen Reduction Reactions. Journal of Power Sources 2011, 196 (5), 2433–2444.

[10] Antolini, E. Palladium in Fuel Cell Catalysis. Energy & Environmental Science 2009, 2 (9), 915.

[11] Salvador-Pascual, J. J.; Citalán-Cigarroa, S.; Solorza-Feria, O. Kinetics of Oxygen Reduction Reaction on Nanosized Pd Electrocatalyst in Acid Media. Journal of Power Sources 2007, 172 (1), 229–234.

[12] Wang, W.; Zheng, D.; Du, C.; Zou, Z.; Zhang, X.; Xia, B.; Yang, H.; Akins, D. L. Carbon-Supported Pd-Co Bimetallic Nanoparticles as Electrocatalysts for the Oxygen Reduction Reaction. Journal of Power Sources 2007, 167 (2), 243–249.

[13] Cheng, L.; Zhang, Z.; Niu, W.; Xu, G.; Zhu, L. Carbon-Supported Pd Nanocatalyst Modified by Non-Metal Phosphorus for the Oxygen Reduction Reaction. Journal of Power Sources 2008, 182 (1), 91–94.

[14] Zhang, L.; Lee, K.; Zhang, J. The Effect of Heat Treatment on Nanoparticle Size and ORR Activity for Carbon-Supported Pd–Co Alloy Electrocatalysts. Electrochimica Acta 2007, 52 (9), 3088–3094.

[15] Stamenkovic, V. R.; Fowler, B.; Mun, B. S.; Wang, G.; Ross, P. N.; Lucas, C. A.; Markovic, N. M. Improved Oxygen Reduction Activity on Pt3Ni (111) via Increased Surface Site Availability. Science 2007, 315 (5811), 493–497.

[16] Wang, Y.; Sun, D.; Chowdhury, T.; Wagner, J. S.; Kempa, T. J.; Hall, A. S. Rapid Room-Temperature Synthesis of a Metastable Ordered Intermetallic Electrocatalyst. Journal of the American Chemical Society 2019, 141 (6), 2342–2347.

[17] Wang, H.; Abruña, H. D. IrPdRu/C as H2 Oxidation Catalysts for Alkaline Fuel Cells. Journal of the American Chemical Society 2017, 139 (20), 6807–6810.

[18] Rößner, L.; Armbrüster, M. Electrochemical Energy Conversion on Intermetallic Compounds: A Review. ACS Catalysis 2019, 9 (3), 2018–2062.

[19] Innocente, A. F.; Ângelo, A. C. D. Electrocatalysis of Oxidation of Hydrogen on Platinum Ordered Intermetallic Phases: Kinetic and Mechanistic Studies. Journal of Power Sources 2006, 162 (1), 151–159.

[20] Cable, R. E.; Schaak, R. E. Low-Temperature Solution Synthesis of Nanocrystalline Binary Intermetallic Compounds Using the Polyol Process. Chemistry of Materials 2005, 17 (26), 6835–6841.

[21] Rodrigues da Silva, M.; Ângelo, A. C. D. Synthesis and Characterization of Ordered Intermetallic Nanostructured PtSn/C and PtSb/C and Evaluation as Electrodes for Alcohol Oxidation. Electrocatalysis 2010, 1 (2–3), 95–103.

[22] Ong, S. P.; Richards, W. D.; Jain, A.; Hautier, G.; Kocher, M.; Cholia, S.; Gunter, D.; Chevrier, V. L.; Persson, K. A.; Ceder, G. Python Materials Genomics (Pymatgen): A Robust, Open-Source Python Library for Materials Analysis. Computational Materials Science 2013, 68, 314–319.

[23] Davis, R. E.; Horvath, G. L.; Tobias, C. W. The Solubility and Diffusion Coefficient of Oxygen in Potassium Hydroxide Solutions. Electrochimica Acta 1967, 12 (3), 287–297.

[24] CRC Handbook of Chemistry and Physics, 66th ed.; Weast, R. C., Ed.; CRC Press: Boca Raton, FL, 1986.

[25] Jiang, L.; Hsu, A.; Chu, D.; Chen, R., Size-Dependent Activity of Palladium Nanoparticles for Oxygen Electroreduction in Alkaline Solutions. J Electrochem Soc 2009, 156.

[26] Wang, Y.; Sun, D.; Chowdhury, T.; Wagner, J. S.; Kempa, T. J.; Hall, A. S. Rapid Room-Temperature Synthesis of a Metastable Ordered Intermetallic Electrocatalyst. Journal of the American Chemical Society 2019, 141 (6), 2342–2347.

[27] Predel, B. Pd-Sb (Palladium-Antimony). In Ni-Np – Pt-Zr; Springer-Verlag; pp 1–2.

[28] Singh, R. K.; Rahul, R.; Neergat, M. Stability Issues in Pd-Based Catalysts: The Role of Surface Pt in Improving the Stability and Oxygen Reduction Reaction (ORR) Activity. Physical Chemistry Chemical Physics 2013, 15 (31), 13044.

[29] Solomun, T. The Role of the Electrolyte Anion in Anodic Dissolution of the Pd(100) Surface. Journal of Electroanalytical Chemistry and Interfacial Electrochemistry 1991, 302 (1–2), 31–46.

[30] Rand, D. A. J.; Woods, R. A Study of the Dissolution of Platinum, Palladium, Rhodium and Gold Electrodes in 1 M Sulphuric Acid by Cyclic Voltammetry. Journal of Electroanalytical Chemistry and Interfacial Electrochemistry 1972, 35 (1), 209–218.

[31] L. Lutterotti, S. Matthies and H. -R. Wenk, "MAUD (Material Analysis Using Diffraction): a user friendly {Java} program for {Rietveld} Texture Analysis and more", Proceeding of the Twelfth International Conference on Textures of Materials (ICOTOM-12), Vol. 1, 1599, (1999).

Hamdan Alghamdi

SABIC Corporate Research and Development Center at KAUST
Permanent Mailing Address: P.O. Box (4545-4700) Thuwal, Saudi Arabia 23955-6900
Mobile: KSA : +966-542229622 USA: +1-443-635-9833 Email: hamdan@ghamdi.org

EDUCATION

Texas A&M University, College Station, TX — Aug. 16th 2013
Bachelor of Science in **Chemical Engineering**
Minors in Chemistry and Mathematics

Johns Hopkins University, Baltimore, MD — Exp. May, 2019
Master's of Science in Engineering (**Chemical Engineering**)

EXPERIENCES

SABIC Corporate Research and Development (CRD), KAUST, Saudi Arabia - Research Engineer, Fundamental Catalysts — March 2014 – Present

SABIC Technology Center, Houston, TX - Intern — September - December 2013

Ar-Razi (SABIC Affiliate), Al-Jubail Industrial City, KSA - *Intern* — May - July 2011

PUBLICATIONS AND PATENTS

Study of the modes of adsorption and electronic structure of hydrogen peroxide and ethanol over TiO_2 rutile (110) surface within the context of water splitting, H Alghamdi, H Idriss, Surface Science 669, 103-113 — 2018

Up-conversion luminescence coupled to plasmonic gold nanorods for light harvesting and hydrogen production, H AlGhamdi, K Katsiev, AK Wahab, J Llorca, H Idriss, Chemical Communications 53 (97), 13051-13054, — 2017

Mechanism of Ethanol Photo-oxidation on Single-Crystal Anatase TiO_2(101), K Katsiev, *et. al.* , J. Phys. Chem. C, 2017, 121 (5), pp 2940–2950 — 2017

[Poster] Density Functional Theory (DFT) Study of Ethanol and H_2O_2 Adsorption and Reactions on TiO_2 Rutile (110) Surface, International Conference of Applied Chemistry (ICAC), King Abdulaziz University, Jeddah, Saudi Arabia — 2015

[Patent Application] Hydrogen Production Using Hybrid Photonic-Electronic Materials, USPO 15756099 — 2018

[Patent Application] Metal Deposition Using Potassium Iodide for Photocatalysts Preparation, USPO 15528855 — 2017

HONORS AND AWARDS

SABIC Higher Education Scholarship Recipient, SABIC — Aug. 2017
SABIC Merit Award Recipient, SABIC — '09, '10, '11
Dean's Honor Roll, Texas A&M University — Spring '11
Distinguished Student Award, Texas A&M University — Spring '10 – Fall '10
President's Honor Roll, Texas A&M University — Fall '09 – Fall '10
SABIC Scholarship Recipient, SABIC — Summer 2008